Highly Reactive Prestressed Aluminum under High Velocity Impact Loading: Processing for Improved Energy Conversion

Kevin J. Hill and Michelle L. Pantoya*

Harnessing greater power from metal particle combustion requires engineering the core-shell particle structure to more rapidly release stored chemical energy upon ignition. This study examines the metallurgical process of prestressing to increase the strain inside aluminum (Al) particles, then links increased strain to altered reaction mechanisms under high velocity impact. Results show that the quenching rate during prestressing changes the Al reaction mechanism. At faster quenching rates (900 K min^{-1}), roughly 50% of the interfacial surface between the Al core and Al$_2$O$_3$ shell delaminates based on a model developed to understand the measured strain. Without core reinforcement, the shell fractures readily upon impact causing dramatically increased ignition sensitivity (measured in terms of pressurization rate) and reactivity (measured in terms of flame spreading). For slower quenching rates (200 K min^{-1}), the core-shell interface remains intact but strain in the particle increases by an order of magnitude. In addition, elastic stiffness in the shell may increase during prestressing. Increased elastic stiffness can effectively reduce ignition sensitivity and higher strain may contribute energy toward the nearly 40% increase in reactivity for the slower quenched aluminum powder. These results establish a link between altering mechanical properties of particles and their ignition and reactivity under dynamic loads.

1. Introduction

As a solid fuel, aluminum (Al) is of great interest because of its high (85 GJ m^{-3}) stored chemical energy. Aluminum particles are a composite of an amorphous aluminum oxide (Al$_2$O$_3$) shell that is about 4 nm thick and encompasses a crystalline Al core. The Al$_2$O$_3$ shell has a high melting temperature (2345 K) and acts as a diffusion barrier that limits Al energy release rates. Several methods have been proposed to increase diffusion rates, including reducing particle size,[1,2] changing shell properties,[3,4] leveraging surface reactions on the alumina shell,[5] and myriad more. Prestressing induces a permanent, compressive strain via annealing and quenching[6] and is a new approach for altering the core-shell properties of an Al particle, thereby affecting its

reaction mechanism and energy release behavior.[7–11] Desirable stresses are compressive in the shell and affect reactivity not by adding additional energy that can be released during combustion but instead by altering the oxide shell dynamics and therefore reaction mechanism during combustion.

Under thermal initiation, compressive stresses in the shell lead to delayed shell failure in nano- and small micron-scale Al particles during combustion.[8–11] The delay allows more of the core aluminum to melt (e.g., melting temperature, 933 K), thereby increasing the amount of molten core released once the shell fractures. With appropriate ignition conditions (i.e., high heating rate), the shell spallates when the core is fully molten, causing aerosolization and dispersion of the molten core and increased reaction rates and energy transport.[12] The reaction mechanism described by this melt-dispersion oxidation process is called the melt-dispersion mechanism (MDM), and it is a mechanochemical way of thinking about the oxidation dynamics of the core-shell particle system.[8–12]

Consolidated aluminum powder is often used as a structural reactive material such that ignition may not be from thermal but instead from mechanical (i.e., impact) stimuli. A structural reactive material not only serves as a high-strength structural material (e.g., aluminum) but can also be converted from a consolidated structure into a large surface area dispersed powder that can be ignited to produce a high intensity blast. Under impact ignition conditions, the consolidated material pulverizes into fragments that are then reactive. Smaller fragments with a higher surface area promote diffusion oxidation reactions that are controlled by the interfacial area between fuel and surrounding oxidizer. On a particle scale, the Al$_2$O$_3$ shell is not pristine but fractured from the impact event. Therefore, under impact ignition, molten Al may not have time to accumulate prior to dispersion and oxidation, and MDM may not be activated because the shell is breached upon impact.

It is not clear how annealing and quenching Al powder would affect Al reactivity under high velocity impact ignition events. The added strain energy from prestressing may spur reactivity by elevating the energy state of the powder. Other research suggests that the elastic stiffness of amorphous alumina may

Dr. K. J. Hill, Dr. M. L. Pantoya
Department of Mechanical Engineering
Texas Tech University
Lubbock, TX 79409, USA
E-mail: michelle.pantoya@ttu.edu

The ORCID identification number(s) for the author(s) of this article can be found under https://doi.org/10.1002/adem.201900492.

ADVANCED
SCIENCE NEWS
www.advancedsciencenews.com

ADVANCED
ENGINEERING
MATERIALS
www.aem-journal.com

increase upon annealing and quenching.[13] An increased elastic stiffness of the shell could resist impact energy and allow more of the core to melt prior to oxidation. Also, physical processes such as delamination between the core and shell has previously been proposed to occur as a result of prestressing.[14] Delamination separates the core from the shell, thereby weakens the shell by removing its reinforcement under impact. All of these thermomechanical and physical alterations within the core-shell particle associated with prestressing are hypothesized to affect the reactive properties of the particle when subjected to high strain rate ignition, such as high velocity impact.

This study examines the reactive response of prestressed Al powder consolidated into projectiles under high velocity impact ignition conditions. The objective is to examine the influence of prestressing on pressurization and flame spreading upon impact and identify unique reaction mechanisms linked to altered particle properties. The objective is accomplished by annealing and quenching Al powder at prescribed rates, pressing the powder into pelletized projectiles, and launching the projectiles at high velocities ($>800\,\mathrm{m\,s^{-1}}$). Dilatational strain of the Al powder is measured using synchrotron XRD. Pressurization rate and flame spreading are related to energy release during and after impact and are key parameters that characterize energy release rate and overall reactivity of the prestressed compared with untreated Al powder, respectively.

2. Experimental Section

2.1. Aluminum Prestressing: Annealing and Quenching Methods

Methods for prestressing metals involve annealing Al powder to an elevated temperature, holding at the annealing temperature for a short duration (i.e., ≈10 min), followed by quenching to room temperature.[6] Two different cooling methods to achieve different quenching rates were investigated. All experiments used the same starting micron-scale Al powder with a 3–4.5 µm average diameter and a 4 nm amorphous Al_2O_3 passivating shell (i.e., 98 wt% Al and 2 wt% Al_2O_3) supplied by Alfa Aesar (Ward Hill, MA). In the first method, the Al powder was annealed in a controlled thermal environment using a Q800 Dynamic Mechanical Analyzer, DMA (TA Instruments). Annealing occurred in an air atmosphere at a heating rate of $10\,\mathrm{K\,min^{-1}}$ to 573 K (300 °C) and held for 10 min. Cooling to 298 K (25 °C) with liquid nitrogen approximated lumped capacitance quenching at an average of $200\,\mathrm{K\,min^{-1}}$. After annealing and quenching in this way, this powder was referred to as prestressed aluminum (i.e., PS Al).

In the second method, approximately 1 g of Al powder was annealed and quenched in a custom-built steel chamber described previously.[14] Annealing was accomplished using a Ney Vulcan 3-130 bake-out furnace under the same heating conditions as the DMA. The powder was sealed within a chamber that cools through immersion in a liquid solution composed of 78.6 wt% water, 9.4 wt% NaCl, 4.1 wt% Dawn blue dish soap, and 7.9 wt% Simple Green, each ingredient was designed to improve an aspect of heat transfer. Using a solution of salt water decreased the liquid heat capacity and adding dish soap inhibited boiling and reduced surface tension of the mixture while the

surfactant improved wetting and thus heat transfer. The chamber sealed with a high temperature silicone O-ring and contained a K-type thermocouple to directly measure the temperature of the powder throughout the quenching process. In this system, the quenching fluid never came in direct contact with the powder. The average quenching rate was $900\,\mathrm{K\,min^{-1}}$. After annealing and quenching in this way, this powder was referred to as super-quenched aluminum (SQ Al) because of the nearly order of magnitude increase in the quenching rate.

2.2. Microstructural Analysis

The microstructure of the polycrystalline Al core particle was analyzed using transmission electron microscopy (TEM). Because the particles were micrometer size, a thin (≈100 nm) slice of the Al particle was milled to electron transparency for TEM lattice imaging using a focused ion beam (FIB) cross-sectioning technique with a Hitachi NB 5000 focused ion and electron beam (dual-beam FIB-SEM) system. Then, the FIB grid mounted on the FIB sample holder was removed from the FIB-SEM system and was compatible with the TEM sample holder such that the thinned Al sample was inserted directly into a Hitachi H-9500 high-resolution TEM for imaging analysis. Details of this procedure were reported in the study by McCollum et al.[15]

2.3. Mixture Preparation

The UN Al, PS Al, and SQ Al were mixed with a binder to aid in consolidation of the projectile. The binder is 1 wt% polyvinylidene fluoride (PVDF) (Sigma Aldrich, St. Louis, MO). To dissolve PVDF and achieve a well-mixed slurry, PVDF and Al were mixed with 1-methyl-2-pyrrolidinone (NMP) and sonicated using a Misonix Sonicator 3000 for 4 min in a programmed cycle of 10 s on/off to prevent thermal energy buildup during mixing. The suspensions were placed in a Pyrex dish and allowed to dry for 48 h in a fume hood on a hot plate set to 358 K (85 °C). Upon retrieval, all powders were sieved through 325 mesh using a grounded brush to break up large agglomerates. The powder was pressed using a hydraulic press into 9.5 mm diameter by 9.5 mm long right circular cylinders at a theoretical maximum density (TMD) of 85% with masses of $1600 \pm 10\,\mathrm{mg}$.

2.4. High-Velocity Impact-Initiation Testing System (HITS)

Figure 1 schematically illustrates the high-velocity impact-initiation testing system (HITS) that includes a .410 caliber powder gun to launch projectiles into an instrumented catch chamber. The projectiles impact a modular, hardened steel anvil, fragment, and combust. A dynamic pressure sensor (PCB Piezotronics 101A06 sensors) positioned 1 cm down the centerline from the anvil recorded pressure at 500 MHz. Two high speed cameras (a Phantom v710 color camera and a Phantom v2512 monochrome camera) recorded both a macroscopic view of the entire catch chamber (at 49 000 fps) and a detailed view of the anvil (at 460 000 fps). The cameras were positioned perpendicular to the direction of projectile motion and aligned with the side viewing window (not shown in Figure 1). The window was made of 1.5 cm polycarbonate to prevent blowout. A white sheet of
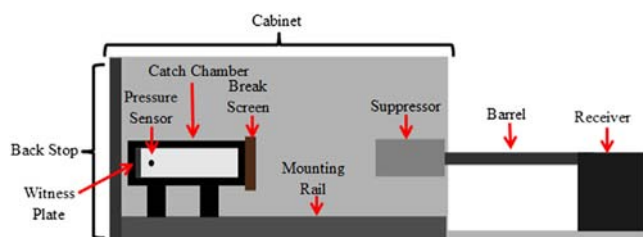
**ADVANCED
SCIENCE NEWS**

www.advancedsciencenews.com

**ADVANCED
ENGINEERING
MATERIALS**

www.aem-journal.com

Figure 1. Schematic of HITS apparatus. HITS apparatus includes .410 caliber powder gun receiver and barrel coupled with a suppressor that is housed in a cabinet that also includes the catch chamber with view port, break screen, pressure sensors, and steel anvil.

Table 1. Average pressurization rate and average flame spread rate for impact and after-blast.

Material	Impact velocity [m s^{-1}]	Impact pressurization rate [MPa ms^{-1}]	After blast pressurization rate [MPa ms^{-1}]	Flame spread rate [m s^{-1}]
UN Al	880	35.6	4.3	158
	1150	45.0	3.9	334
PS Al	860	5.2	5.1	58
	1260	70.7	5.6	380
SQ Al	910	40.1	5.8	356
	1200	96.3	5.8	402

paper was placed along the back of the chamber to assist in projectile visualization and flame tracking during post-processing. The projectile passed through a break screen composed of thin paper with thin pieces of aluminum foil (biased with a 9V battery) to trigger the cameras and data acquisition system (a Picoscope 5444B). A minimum of five tests were performed for each impact velocity and powder prestressing method. The high-speed cameras enabled measurements of impact velocity and flame spreading after impact. The pressure sensor enabled measurement of pressurization rate.

The data are processed from still frame images in two ways: 1) to assess the projectile impact velocity from location of the projectile as a function of time and 2) according to light intensity corresponding to ignition and flame spreading. Ignition was determined from first light. Flame spreading after impact was analyzed using Phantom Control Center (PCC) software. The software allowed the user to input a pixel to length calibration and track the location and time of an object or gradient in light intensity in the field of view. Flame spreading was defined as the rate at which the cloud of particles combusts (either radially along the anvil or axially through the chamber). Two types of flame spreading were observed: a rapid radial (vertical) spread corresponding to projectile impact on the anvil and a slower axial (horizontal) spread through the chamber away from impact. The radial flame spreading ended before the axial flame spreading began. These data are exported and used to create a linear (steady state) plot of position as a function of time. A best fit line was plotted to obtain the flame spread rate. The axial flame spread rate was steady state, with R^2 values greater than 95%. Five experiments for each aluminum powder were performed and the average flame spread rate is reported in **Table 1**. Uncertainty was estimated as 10% from the standard deviation in the flame spread rates measured from multiple samples.

Pressurization rate from the pressure sensor during impact and after-blast were extracted from the raw pressure data by applying a 10 000 Hz low pass filter to remove high frequency noise and measure the maximum and minimum pressure values (and their corresponding time stamps) during impact and during after-blast flame spreading. The minimum value must also occur just prior to significant pressurization and is further defined as the first point to reach 1% of the maximum pressure during the event. The low pass filter removed most of the high frequency noise generated by shock wave and pressure reflections within the catch chamber. However, some oscillatory noise remained,

generating uncertainties of $\approx$100 kPa during impact and $\approx$10 kPa during after-blast, which resulted in shot-to-shot uncertainties of <10%.

3. Results

Changes in quenching rates during powder prestressing may alter the microstructure of Al particles, with faster quenching rates leading to shell delamination from the particle core and slower quenching rates increasing hoop stress in the shell. The 3–4.5 μm diameter Al particles are annealed to 573 K, then quenched at different rates: 200 K min^{-1} (prestressed, PS Al) and 900 K/min (super-quenched, SQ Al). The Al particles are mixed with 1 wt% polyvinylidene fluoride (PVDF) and pressed into pellets. The pellet projectiles are launched from a powder gun at speeds ranging from 850 to 1200 m s^{-1}, and pressurization rate is measured during impact, and pressurization rate and flame spreading are measured during after-blast.

Movie files representative of the impact events are included in Supporting Information. Because each impact event is phenomenologically similar, a single video representing **Figure 2**A and a single video representing Figure 2B,C are provided. Figure 2 shows still frame images of impact for UN Al projectiles travelling at 900 m s^{-1} as a representative case. All powder treatments at all impact velocities demonstrate similar impact behavior: radial flame spread followed by axial flame spread through the chamber. First observable light emission (i.e., ignition time) from the projectile occurs between impact and the next frame of video corresponding to a difference of less than 6.51 μs for UN Al, PS Al, and SQ Al, respectively, and is visible across the entire impact surface. Therefore, ignition time upon impact is <6.51 μs for all materials examined.

In Figure 2, it is unclear if comminution occurs prior to flame spreading. Fragmentation may be masked by the light emitted from reaction such that ignition appears to occur directly upon projectile impact. The ignition mechanism may include the following processes: strain-induced mixing with the binder, pore collapse within the porous projectile (e.g., 15% porosity), and reaction with oxygen from the surrounding environment or fluorine from PVDF. All these processes promote hot spots that trigger ignition and energy generation.
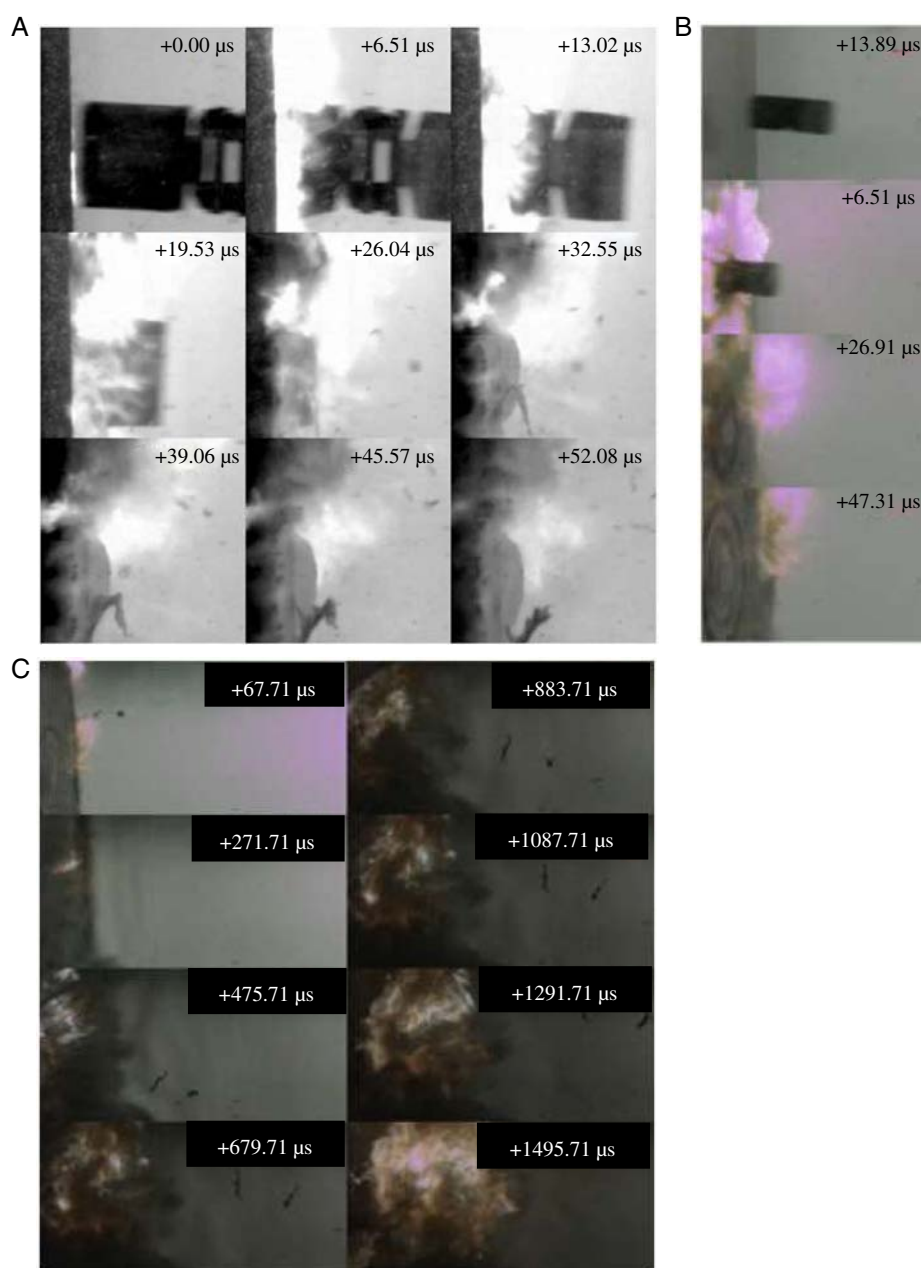
Figure 2. Still frame movie images from UN Al projectile impact at 900 m s^{-1}. A) Detailed view from impact to 52 µs. Note from left to right at 0.0 µs: impact anvil, pellet, and wad. B) Macroscopic view time stamped from impact. Note radial propagation waves are seen on the anvil at 26.91 and 47.31 µs. C) Macroscopic view of flame spreading from impact to 1.5 ms.

Table 1 shows pressurization rate during impact as well as pressurization rate and flame spread rate during after-blast. During impact, there are large differences in pressurization rate both between impact velocities for the same prestressing conditions and between the same impact velocities at different prestressing conditions. The pressurization rate during impact is an indication of the ignition sensitivity such that PS Al is least sensitive to impact ignition at lower impact velocities with the lowest pressurization rate. In contrast, SQ Al is the most sensitive to impact ignition with the highest pressurization rate at low and high impact velocities.

In the after-blast stage of reaction, differences in pressurization rates are small between different impact velocities for the same prestressing condition, although the differences between prestressing conditions are quite large. For all impact velocities, stress altered powder exhibit higher pressurization rates in the after-blast indicating that in the deflagration zone of reaction, stress altered powder is more reactive. Flame spreading during

**ADVANCED
SCIENCE NEWS**

www.advancedsciencenews.com

**ADVANCED
ENGINEERING
MATERIALS**

www.aem-journal.com

deflagration follows a similar trend as pressurization rate during impact. At the lower impact velocity, SQ Al flame spreading is 125% faster than the UN Al, but the PS Al is 63% slower than UN Al. At the higher impact velocity, the SQ Al is 20% faster than the UN Al, and the PS Al becomes faster than the UN Al by 14%. The flame spreading behavior is closely linked with impact pressurization rate, such that higher pressurization rate under impact correlates with faster flame spreading.

Synchrotron radiation X-ray diffraction (SR-XRD) experiments were performed at the Advanced Light Source facility at Lawrence Berkeley National Laboratory on beamline 12.3.2 using a micron-focused synchrotron X-ray beam for all Al powders examined here. Measurements from this beamline quantify dilatational strain from Al powder subjected to various annealing and quenching treatments.[9,15–19] **Table 2** shows the average measured dilatational strain for each sample. The UN Al powder exhibits nearly zero dilatational strain, but there is an order of magnitude increase in dilatational strain for prestressed materials regardless of the quenching rate.

Figure 3 shows TEM images of a slice from a 10 µAl particle to reveal the inner polycrystalline core for both UN Al and PS Al. The slice is prepared using a focused ion beam (FIB) to mill the particle to electron transparency. The analysis is performed to investigate changes in grain and grain boundary microstructure that may occur due to prestressing. The TEM analysis shows no significant changes in grain morphology that result from prestressing, indicating that the main alteration is attributed to the volumetric strain measured as a dilatational strain using SR-XRD.

4. Discussion

One interesting observation from Table 1 is the difference in reactivity at different impact velocities between samples. In all cases, when comparing samples at the same impact velocity, SQ Al is more ignition sensitive (higher pressurization rate) and demonstrates greater overall reactivity during deflagration (faster flame spreading). The flame spread rate and the pressurization rate during impact mirror each other and give insight into the reactivity of these particles at different quenching rates. During the lower velocity impact, PS Al underperforms UN Al in pressurization rate (86% decrease), while SQ Al demonstrates higher pressurization rate (13% increase). At the higher impact velocity, both PS Al and SQ Al outperform UN Al in pressurization rate (57% and 114%, respectively). These differences may be explained by different shell mechanics at impact that affects particle ignition and deflagration.

The difference between samples is the dilatational strain (Table 2) with negligible variations in grain microstructure

Table 2. Average dilatational strain in Al powder measured using SR-XRD. Note that UN Al and PS Al data are from ref. [15], and SQ Al is from ref. [14].

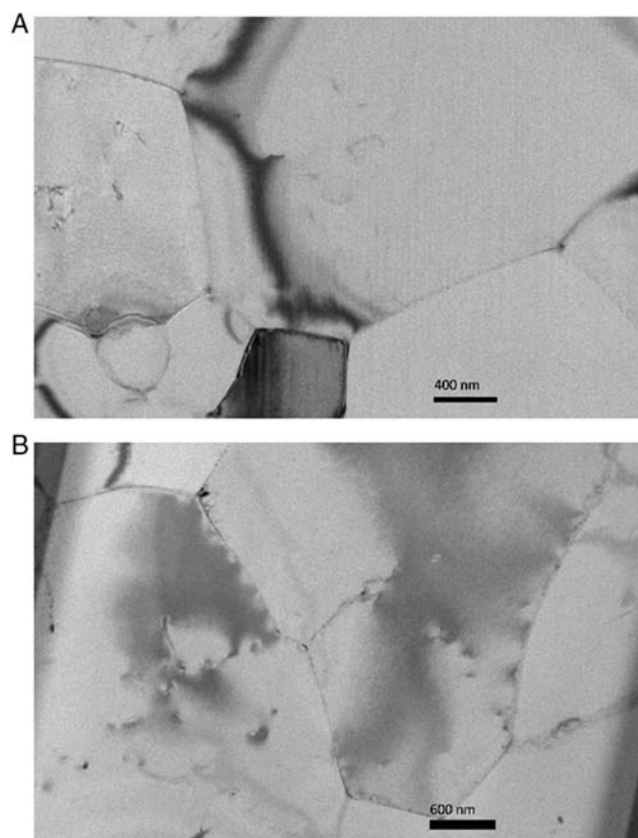| Material	Dilatational strain
UN Al	1.5×10^{-6}
PS Al	9.23×10^{-5}
SQ Al	5.7×10^{-5}

Figure 3. Images from FIB-TEM analysis of polycrystalline microstructure of A) UN Al and B) PS Al. Images show no significant changes in grain morphology or grain boundary microstructure. Note HV = 300 kV for both images and Direct Mag. × 1200 and × 8000 for UN Al and PS Al, respectively.

(Figure 3). Previous work modeled ≈50% delamination of the Al core from the Al_2O_3 shell for SQ Al[14] assuming no quenching-induced shell defects. With elevated strain, PS Al has a large compressive hoop stress in the shell but no delamination between particle core and shell. For SQ Al, delamination between core and shell may facilitate shell failure during impact because the Al core no longer reinforces the shell, thereby promoting shell fracture and core exposure leading to ignition and reaction. For SQ Al, delamination reduces the oxidation barrier, while the added hoop stress from prestressing (Table 2) intensifies fracture of the shell. It is likely that SQ Al performs similarly at both impact velocities because of the extensive delamination along the core–shell interface. The delaminated structure allows similar oxidation because the impact velocity provides sufficient energy to cause shell failure.

At the lower impact velocity, PS Al shows reduced flame spreading rate and impact pressurization rate compared with UN Al (Table 1). The PS Al pressurization rate in the after-blast stage is higher than UN Al and as the impact velocity increases, the flame spreading differences become smaller, both trends suggest that shell failure is activated and oxidation proceeds in all samples, including UN Al. There may be multiple reasons for the lag in PS Al reactivity at lower impact velocities. For

example, at 860 m s^{-1}, the impact energy may not be sufficient to overcome the order of magnitude increased hoop stress in the shell (Table 2) and activate shell failure. At 860 m s^{-1}, the total kinetic energy of the projectile is 592 J, while at 1260 m s^{-1}, the kinetic energy is 1270 J. Each 3.5 μm Al particle has approximately 0.224 nJ of kinetic energy at 860 m s^{-1} and 0.481 nJ of kinetic energy at 1260 m s^{-1}, indicating that the kinetic energy required to overcome the hoop stress in PS Al under impact lies between 0.224 and 0.481 nJ. Another possibility is that the amorphous structure of the alumina shell changes during annealing and quenching leading to changes in the mechanical properties of the shell. Tane et al.[13] studied the formation of nanovoids in amorphous alumina films through annealing that retained their amorphous phase but increased the alumina density by 4%. They found that the elastic stiffness of alumina increased by up to 28% with annealing, suggesting that more stress is needed for PS Al to create the same amount of strain in UN Al. Molecular dynamic simulations revealed that an increase in stable AlO_6 basic units and the change in ring distribution led to the increases in elastic stiffness and density. Tane et al.[13] also showed that changes in density and elastic stiffness occur quickly during annealing (i.e., less than 1 h annealing time) and increase with quenching rate. They studied that Al_2O_3 films reinforced on silicon substrates similar to the PS Al with alumina shells reinforced by the Al core. Increased elastic stiffness in the shell may strengthen the shell aiding in retarding impact ignition enough to produce lower peak pressure and pressurization rate for PS Al particles compared with UN Al. In contrast, SQ Al would not experience similar impact impedance due to delamination between the particle core and shell.

Two mechanisms may contribute to the PS Al reduced pressurization rate upon impact: 1) higher particle strain (Table 2) that requires greater activation energy for ignition and 2) altered shell structure during annealing that increases shell stiffness thus requiring greater ignition energy. Flame spreading in the after-blast, deflagration region is also reduced for PS Al under low impact velocity conditions indicating that burning behavior is linked to ignition sensitivity. The SQ Al particles show reduced dilatational strain from PS Al, although SQ Al is prepared at a faster quenching rate than PS Al. The reduced strain may be attributed to stress relaxation due to delamination at the core–shell interface. An unsupported, delaminated shell is more impact ignition sensitive as seen in Table 1 for SQ Al with the highest pressurization rates in both impact and after-blast regions of reaction and faster flame spreading rates for both impact velocities. Both strain-altered powders exhibit unique reaction dynamics linked to different reaction mechanisms associated with their elevated dilatational strain.

5. Conclusion

Annealing and quenching aluminum (Al) powders alter their strain and affect their mechanism of reaction under high velocity impact ignition conditions. This study showed that at faster quenching rates (900 K min^{-1}), the increase in particle strain is not as high as theoretically predicted. A reduction in measured strain may result from strain relaxation due to delamination at the core–shell particle interface. An analytical model predicts 50% of the interfacial surface between the Al core and Al_2O_3 shell delaminates. Without core reinforcement, the shell fractures readily upon impact causing dramatically increased ignition sensitivity (shown as increased pressurization rate) and overall reactivity (shown as flame spreading). For slower quenching rates (200 K min^{-1}), the core–shell interface remains intact and strain in the particle is increased by an order of magnitude. For the slower quenched particles, elastic stiffness in the shell may also increase such that ignition is delayed. These more impact resistant particles may experience delayed shell failure but exhibit nearly 40% increase in flame spreading rate. Slower quenching produces particles that are more impact resistant but exhibit greater flame spreading at high impact velocities while faster quenching sensitizes particles to impact ignition and enhances flame spreading behavior through a delamination reaction mechanism. Tailoring Al particles via prestressing offers improvement and more control over their ignition and reaction under high strain rate loading such as high velocity impact.

Conflict of Interest

The authors declare no conflict of interest.

[1] W. He, P.-J. Liu, G.-Q. He, M. Gozin, Q.-L. Yan, *Adv. Mater.* **30**, **2018**.

[2] A. Prakash, A. V. McCormick, M. R. Zachariah, *Adv. Mater.* **17**, **2005**.

[3] D. K. Smith, D. K. Unruh, C. C. Wu, M. L. Pantoya, *J. Phys. Chem. C* **2017**, *121*, 23184.

[4] D. K. Smith, D. K. Unruh, M. L. Pantoya, *J. Phys. Chem. C* **2017**, *121*, 23192.

[5] C. A. Crouse, C. J. Pierce, J. E. Spowart, *Appl. Mater. Interfaces* **2010**, *2*, 2560.

[6] J. R. Davies, *Powder Metallurgy Processing. Aluminum and Aluminum Alloys*, A. S. M. International, Materials Park, OH, p. 275, **1993**.

[7] B. Dikici, M. L. Pantoya, V. I. Levitas, *Combust. Flame* **2010**, *157*, 1581.

[8] V. I. Levitas, B. Dikici, M. L. Pantoya, *Combust. Flame* **2011**, *158*, 1413.

[9] V. I. Levitas, J. McCollum, M. L. Pantoya, *Sci. Rep.* **2015**, *5*, 7879.

[10] V. I. Levitas, J. McCollum, M. L. Pantoya, N. Tamura, *J. Appl. Phys.* **2015**, *118*, 094305.

[11] J. E. Hatch, *Aluminum: Properties and Physical Metallurgy*, American Society for Metals, Ohio **1984**.

[12] V. I. Levitas, B. W. Asay, S. F. Son, M. L. Pantoya, *J. Appl. Phys.* **2007**, *101*, 083524.

[13] M. Tane, S. Nakano, R. Nakamura, H. Ogi, M. Ishimaru, H. Kimizuka, H. Nakajima, *Acta Mater.* **2011**, *59*, 4631.

[14] K. J. Hill, N. Tamura, V. I. Levitas, M. L. Pantoya, *J. Appl. Phys.* **2018**, *124*, 115903.

[15] J. McCollum, D. K. Smith, K. J. Hill, M. L. Pantoya, J. Warzywoda, N. Tamura, *Combust. Flame* **2016**, *173*, 229.

[16] J. McCollum, M. L. Pantoya, N. Tamura, *Acta Mater.* **2016**, *103*, 495.

[17] V. I. Levitas, J. McCollum, M. L. Pantoya, N. Tamura, *Combust. Flame* **2016**, *170*, 30.

[18] M. Kunz, N. Tamura, K. Chen, A. A. MacDowell, R. S. Celestre, M. M. Church, S. Fakra, E. E. Domning, J. M. Glossinger, J. L. Kirschman, G. Y. Morrison, D. W. Plate, B. V. Smith, T. Warwick, H. A. Padmore, E. Ustundag, V. V. Yashchuk, *Rev. Sci. Instrum.* **2009**, *80*, 035108.

[19] N. Tamura, in *Strain and Dislocation Gradients from Diffraction: Spacially-Resolved Local Structure and Defects* (Eds: R. Barabash, G. Ice), Imperial College Press, Covent Garden, London, p. 125, **2014**.